Switched-Beam Endfire Planar Array With Integrated 2-D Butler Matrix for 60 GHz Chip-to-Chip Space-Surface Wave Communications

Switched-Beam Endfire Planar Array With Integrated 2-D Butler Matrix for 60 GHz Chip-to-Chip Space-Surface Wave Communications

Prabhat Baniya, *Student Member, IEEE,* and Kathleen L. Melde, *Fellow, IEEE*

***Abstract*—A 2-D Butler matrix feed network is designed, implemented, and integrated with a 60-GHz 2 × 2 circular patch planar array for chip-to-chip communications. The realized antenna module is a thin multilayer microstrip structure with a footprint small enough to fit over a typical multicore chip. The network enables end-fire (azimuthal) scan of the array main beam in the four diagonal directions, which is demonstrated for the first time here. The antenna module provides a seamless and practical way to achieve reconfigurable interchip communication in multicore multichip (MCMC) systems. A hybrid space-surface wave interconnect is proposed that takes advantage of surface wave coupling. The matrix is a four input, four output i.e., 4 × 4 network consisting of four interconnected quadrature (90°) hybrid couplers. A multi-antenna module (MAM) consisting of five antenna modules that emulates diagonal interchip communication in MCMC systems is fabricated. The simulation and measurement of transmission coefficients between the antenna modules on the MAM are performed and compared.**

***Index Terms*—60 GHz antenna, Butler matrix, chip-to-chip antenna, circular patch, interchip, multicore multichip (MCMC), planar array, reconfigurable, switched beam.**

I. Introduction

RECONFIGURABLE interchip communication in multicore multichip (MCMC) computing systems can be achieved through the use of millimeter wave (mmW) switched-beam antenna arrays connected to CMOS chip routers [1], [2]. Traditionally, the mmW antennas have been used to provide high speed wireless interconnection between the chips to solve the wiring complexity problem in such systems [3]–[7]. The wireless interconnects require the use of transceivers and beamforming networks (BFNs) along with the antennas for data transfer [6], [7]. Beamforming using solid-state phase shifters is not practical at mmW frequencies due to high loss [8]. Pattern reconfiguration at 60 GHz by simply switching array elements on and off has been proposed in [9]. The loss in the switch network will depend largely on the type and number of switches used [10], [11]. Alternatively, the Butler matrix and the Rotman lens have been extensively used as BFNs for linear arrays at 60 GHz [12]–[17]. The BFNs still require one single-pole n-throw (SPnT) switch.

Manuscript accepted December 8, 2018. This work was supported by the National Science Foundation under Grant ECCS-1708458. *(Corresponding author: Prabhat Baniya.)*

The authors are with the Department of Electrical and Computer Engineering, University of Arizona, Tucson, AZ 85721 USA (e-mail: pbaniya@email.arizona.edu; melde@email.arizona.edu).

Digital Object Identifier 10.1109/LAWP.2018.2887259

The scan coverage of an array is determined by the type of the array used [18]. A linear array is capable of only 180° scan coverage using the traditional (1-D) Butler matrix [13]. On the other hand, a planar array can provide 360° scan coverage and is better suited for the chip-to-chip communications in all eight directions [1], [2]. A planar array can be fed by the 2-D Butler matrix, as proposed here, which is a combination of two 1-D Butler matrices. In [19], an eight beam end-fire scanning array using magneto-electric (ME) dipole elements with the 1-D Butler matrix has been demonstrated but the angular coverage is limited to 180°. A BFN based on the 1-D Butler matrix with stacked-patches that scans in two planes is presented in [20] but for broadside scanning. A substrate integrated waveguide (SIW) implementation of the 2-D Butler matrix with a ME dipole planar array is presented in [21] but also for broadside scanning.

In this letter, the 60-GHz circular patch planar arrays with integrated 2-D Butler matrices are proposed to provide both the space and surface wave interconnection. The antenna modules have four diagonal end-fire beams with significant surface wave excitation which helps to increase the power coupling between the chips and improve signal power at large distances. Finally, a link decomposition technique to quantify the relative contribution of space and surface waves is applied.

II. Hybrid Space-Surface Wave Interconnect

The antenna array and feed network at 60 GHz can be made small enough to fit over a multicore chip of a typical size [22] with little to no area overhead and ultimately minimize the chip-to-chip distances, as illustrated in Fig. 1. The arrays must provide communication over these distances, usually several tens of millimeters. Fig. 2 shows how the antenna module can be packaged (surface mounted) over the CMOS chips (which has integrated transceivers and multiple cores). The chips are BGA mounted on the board. By matching the layout and arrangement of the antenna modules to the chips underneath, the substrates and ground planes of each antenna module can be connected together to form an interconnect layer parallel to the PCB board/chips and thus take advantage of the surface wave coupling in addition to the space wave coupling. The SPnT switch can be flip-chip (C4) attached to the feed layer. The transceivers serialize/deserialize the data to be exchanged, and provide the 60 GHz modulated/demodulated signals for transmission/reception by the antennas [23].

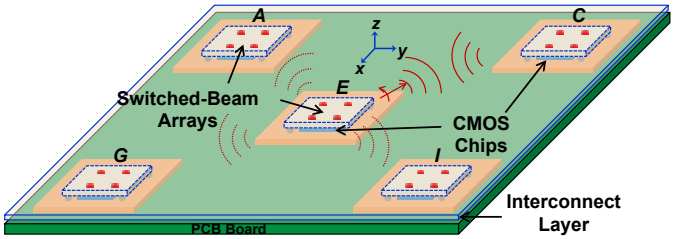

Fig. 1. The antenna modules are packaged on top of multicore CMOS chips. The antenna arrays provide switchable beams in the horizontal plane for reconfigurable chip-to-chip communications [1], [2].

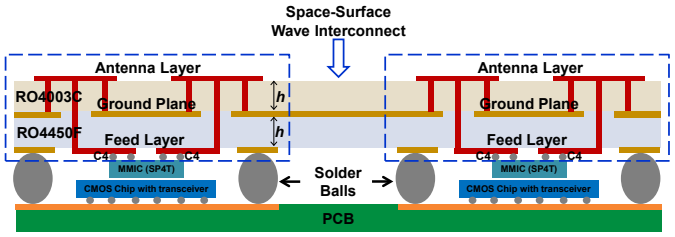

Fig. 2. Detailed side view of Fig. 1 showing the hybrid space-surface wave interconnect for 60-GHz chip-to-chip communications. The multilayer antenna modules are surface mounted on the PCB board over the chips [2].

Figs. 1 and 2 depict how the antenna arrays can be used for interchip communication [1], [2]. The communication is done through the hybrid interconnect layer. Note that in order for a module (e.g., *E* in Fig. 1) to communicate to all its eight adjacent neighbors (only four shown), the array should provide eight beams (i.e., 360° angular coverage in 45° steps). A simpler case of beam scanning in only the diagonal directions with four beams (360° angular coverage in 90° steps) is demonstrated here for the first time. Interchip communication in the diagonal directions can reduce the average hop count and latency in the network [24].

III. 2-D Butler Matrix for Planar Array

A. Working Principle of 2-D Butler Matrix

The four input four output (4 × 4) 2-D Butler matrix with a 2 × 2 planar array is shown in Fig. 3. It provides four switchable diagonal beams in the azimuth plane (end-fire). The interelement phase shifts β_x and β_y in the *x*- and *y*-directions, respectively, required to have the main beam of the planar array [1], [2], [25] sweep along the four diagonal directions i.e., $\phi_0 = 45°, -45°, 135°$, and $-135°$ in the azimuth plane ($\theta_0 = 90°$) are given in Table I.

The 4 × 4 2-D Butler matrix consists of four quadrature (90°) hybrid couplers interconnected to provide a specific phase difference between the output signals for each input excitation. Note that the proposed matrix does not require the use of crossovers and 45° phase shifters. Let us consider the case when port 1 is excited. Fig. 3 shows the signal flow graph. For port 1 excitation, the two arms of the right coupler produce signals $-j/\sqrt{2}$ and $-1/\sqrt{2}$ at the coupler output. The signal $-j/\sqrt{2}$ from the bottom arm is further split by the bottom coupler into signals $-1/2$ at a_4 and $j/2$ at a_3 while the signal $-1/\sqrt{2}$ from the top arm is further split by the top

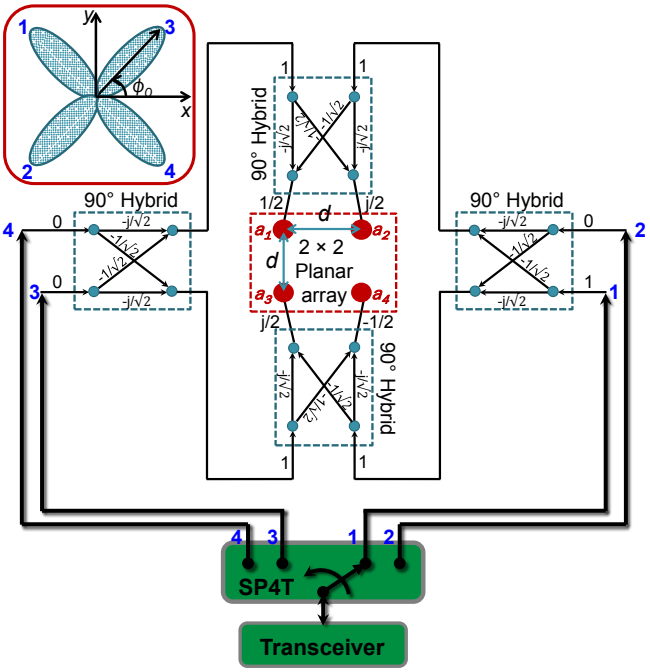

Fig. 3. 4 × 4 2-D Butler matrix for planar array (360° angular coverage in 90° steps). The SP4T switch enables electronic scanning of the array main beam by connecting one of the Butler matrix inputs to the transceiver [2].

TABLE I
Interelement Phase Shifts Required for Main Beam Formation in the Azimuth Plane [1], [2]

Port	ϕ_0	β_x	β_y
1	$+135°$	$+90°$	$-90°$
2	$-135°$	$+90°$	$+90°$
3	$+45°$	$-90°$	$-90°$
4	$-45°$	$-90°$	$+90°$

coupler into signals $j/2$ at a_2 and $1/2$ at a_1. This effectively achieves $\beta_x = +90°$ and $\beta_y = -90°$, and produces the main beam along $\phi_0 = +135°$ (see Table I). Each input port is isolated from the other and there is equal power division at the output ports.

B. Microstrip Implementation of Butler Matrix

The Butler matrix is realized as a feed layer (illustrated in Fig. 2) on a Rogers RO4450F prepreg ($\epsilon_r = 3.52, \tan\delta = 0.004$) [26]. The middle ground plane helps to minimize interference by blocking antenna radiation into the feed layer and CMOS circuits underneath. The 3-D model of the Butler matrix created in high frequency structural simulator (HFSS) is shown in Fig. 4(a). The feed layer resides below the ground plane (hidden). The 100 Ω microstrip lines are used to realize the hybrids [12]. The input and output ports are labeled in Fig. 4(a) and have impedances of 100 Ω and 50 Ω respectively. The input ports *i* = 1 to 4 must be later transformed to 50 Ω for probing (see Section IV). The output ports *j* = 5 to 8 were transformed to 50 Ω using quarter-wave lines so that they can be matched to 50 Ω antenna elements. The vias at the output ports, each have diameter a_f of 0.15 mm and serve to feed

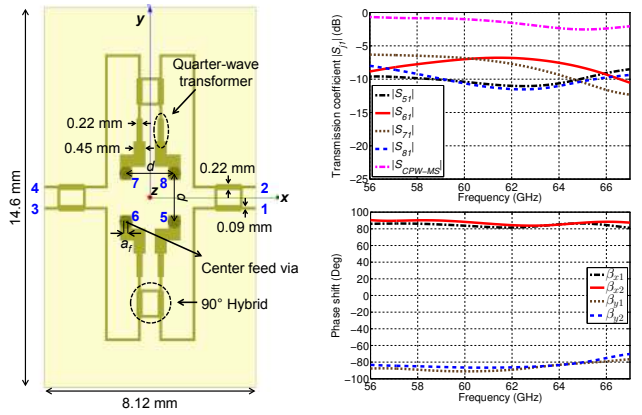

(a) (b)

Fig. 4. (a) 3-D model of the 4 × 4 2-D Butler matrix. (b) Transmission coefficients and interelement phase shifts $(\beta_{x1})_1$, $(\beta_{x2})_1$, $(\beta_{y1})_1$ and $(\beta_{y2})_1$ at the matrix output when port 1 is excited.

the elements. They are separated by distance $d = 1.86$ mm [1], [2].

The S-parameters of the Butler matrix are obtained by performing full wave simulation in HFSS. The simulated reflection coefficient magnitude ($|S_{ii}|$) of the Butler matrix for all identical input ports i is -28 dB at 60 GHz and less than -10 dB across the band (56–67 GHz) indicating a broad impedance match. The transmission coefficients ($|S_{ji}|$) from input port i = 1, to output ports j = 5 to 8, shown in Fig. 4(b), are not equal due to uneven losses. The interelement phase shifts $(\beta_x)_i$ and $(\beta_y)_i$ for port i excitation can be derived from the phase difference between the transmission coefficients as follows.

$$(\beta_x)_i = \begin{cases} (\beta_{x1})_i = (\beta_{a_{2,1}})_i = (\beta_{87})_i = \angle S_{8i} - \angle S_{7i} \\ (\beta_{x2})_i = (\beta_{a_{4,3}})_i = (\beta_{56})_i = \angle S_{5i} - \angle S_{6i} \end{cases} \quad (1)$$

$$(\beta_y)_i = \begin{cases} (\beta_{y1})_i = (\beta_{a_{2,4}})_i = (\beta_{85})_i = \angle S_{8i} - \angle S_{5i} \\ (\beta_{y2})_i = (\beta_{a_{1,3}})_i = (\beta_{76})_i = \angle S_{7i} - \angle S_{6i} \end{cases} \quad (2)$$

For port i = 1 excitation, the interelement phase shifts $(\beta_{x1})_1$, $(\beta_{x2})_1$, $(\beta_{y1})_1$ and $(\beta_{y2})_1$ are plotted in Fig. 4(b). At the design frequency of 60 GHz, it can be seen that $(\beta_{x1})_1 \approx +85°$, $(\beta_{x2})_1 \approx +90°$, $(\beta_{y1})_1 \approx -90°$, and $(\beta_{y2})_1 \approx -85°$. This matches the expected values in Table I within a small $\pm 5°$ margin. Moreover the phase shifts are maintained over a wideband.

IV. Packaging of Multilayer Antenna Module

The selection of the antenna element is driven by the need to maximize horizontal (end-fire) radiation. The 2 × 2 planar array of center fed circular patches with side vias introduced in [1] serves this purpose well. The top (antenna) layer of the 3-D model in Figs. 5(a) and (b) shows the array. The interelement separations, d_x and d_y are both fixed at $d = 1.86$ mm. The ground plane size is 12.34 mm × 14.6 mm but the substrate is extended by 1.27 mm on all sides to meet the copper edge clearance requirement for fabrication. The diameters of the center feed via a_f and four side vias a_s are 0.15 mm each

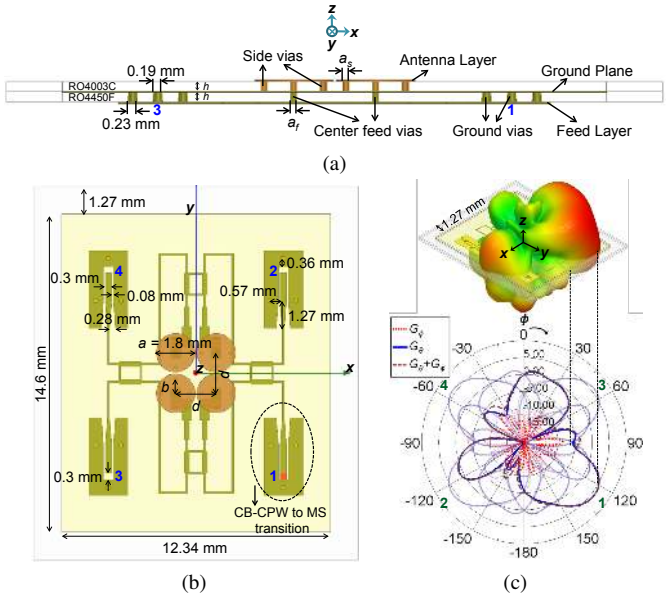

(a) (b) (c)

Fig. 5. 3-D model of the multilayer antenna module. (a) Side view. (b) Top view. (c) Simulated horizontal gain patterns (dB) at 60 GHz: Port 1 ($\phi_0 = +135°$), Port 2 ($\phi_0 = -135°$), Port 3 ($\phi_0 = +45°$), Port 4 ($\phi_0 = -45°$).

and the side vias are located at radial distance $b = 0.67$ mm from the patch center [1]. The antenna layer is printed on a Rogers RO4003C dielectric core ($\epsilon_r = 3.55, \tan\delta = 0.0027$) [27]. The prepreg containing the Butler matrix (feed) layer is then stacked and bonded with the core. The ground plane is sandwiched between the feed and antenna layers. This integrates the Butler matrix of Fig. 4(a) with the array. The realized multilayer antenna module, in Figs. 5(a) and (b), is suitable for an antenna-in-package implementation with the CMOS chips [28]–[31]. The prepreg and the core each have thickness $h = 0.2$ mm with 35 μm copper finish.

To transform the input port impedance, conductor backed coplanar waveguide (CB-CPW) to microstrip (MS) transitions are augmented at the input of the Butler matrix, as shown in Fig. 5(b). The 100 Ω microstrip lines are transformed to the 50 Ω CB-CPW lines by linearly tapering the width and the gap of the interconnecting lines. The side and back traces of each CB-CPW pad are grounded by using three laser vias. The CB-CPW inputs are individually excited to switch the main beam of the module. The simulated insertion loss of the transition is 1 dB at 60 GHz (see Fig. 4(b)). Each port excitation attains a combination of interelement phase shifts given in Table I and produces a main beam in one of the four diagonal directions. The beam switching can be seen in the horizontal gain patterns ($\theta = 90°$) shown in Fig. 5(c). The antenna module has an end-fire main beam with a peak gain of 5.3 dBi at 60 GHz along the diagonal directions (ϕ_0). This gain is with the Butler matrix and CPW transitions included. The highest side lobe level (SLL) is 1.3 dBi. With mutual coupling ignored, the SLLs can be 10 dB below the peak for a uniformly excited 2 × 2 isotropic planar array at the given d [1]. In practice, the SLLs could be reduced by tapering the amplitude distribution at the array feed [25]. The total radiation efficiency of the module is 76% at 60 GHz. The pattern in Fig. 5(c) is more asymmetric

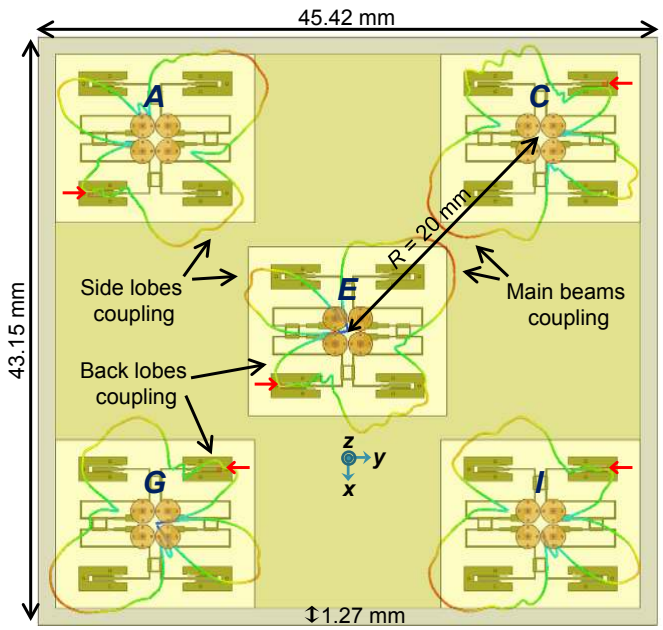

Fig. 6. MAM 3-D model with five antenna modules. The 60 GHz simulated gain patterns (dB) of the modules are overlaid on the MAM.

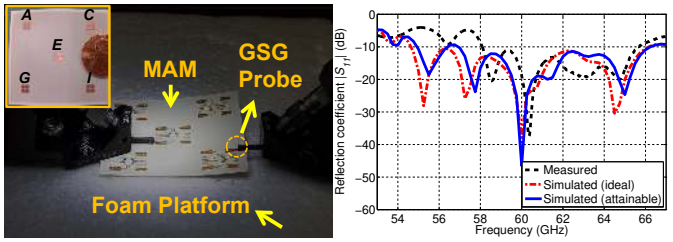

(a) (b)

Fig. 7. (a) Measurement setup of the fabricated MAM prototype. (b) Reflection coefficient (dB) of an antenna module on the MAM.

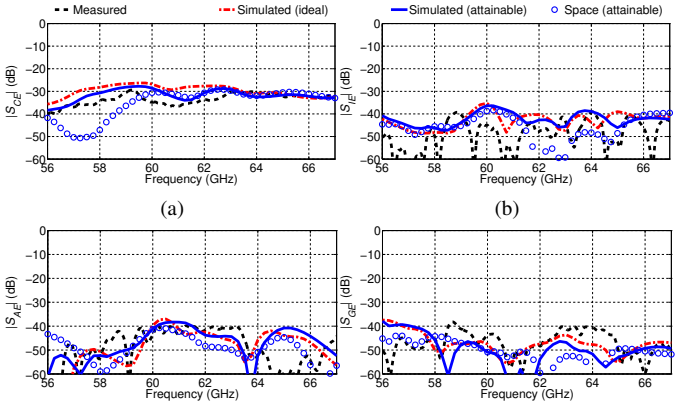

(a) (b) (c) (d)

Fig. 8. Measured and simulated transmission coefficients (dB) between the antenna modules on the MAM. (a) $|S_{CE}|$. (b) $|S_{IE}|$. (c) $|S_{AE}|$. (d) $|S_{GE}|$.

than the array pattern in [1] due to uneven losses in the matrix.

V. Chip-To-Chip Communication in MCMC Systems

A. Antenna Modules in MCMC System

To emulate the chip-to-chip communication scenario of Fig. 1, five antenna modules were put together to form a larger multi-antenna module (MAM), as shown in Fig. 6. The modules are separated by a small interchip diagonal distance of $R = 20$ mm. All antenna modules are identical to the module in Fig. 5(b). The substrates and ground planes of each module are connected together to form an interconnect layer (with a larger common substrate and ground plane). This allows surface wave coupling to occur between the antenna modules [32]–[34], and improve interchip transmission.

Many pairs of chips are expected to communicate concurrently in MCMC systems. Consider the beam configuration shown in Fig. 6, which is representative of a concurrent communication between several chips. The ports (indicated by red arrows) are excited on antenna modules *E* and *C* so that their main beams point at one another. Thus the pair *E*–*C* is referred to as the communicating pair. At the same time, the ports on modules *A*, *G* and *I* are also excited so that their main beams point towards neighboring modules other than module *E* (consider the MAM in Fig. 6 is larger and has more modules around it). The radiation from *A*, *G* and *I* in the direction of *E* contribute to interference and vice versa. The goal is to maximize the radiation between *E*–*C* (communicating pair) while minimizing it between *E*–*A*, *E*–*G* and *E*–*I* (interfering pairs). The overlaid gain patterns show the differences in the radiation coupling between the pairs.

B. Reflection and Interchip Transmission Coefficients

The fabricated PCB prototype of the MAM with the measurement setup is shown in Fig. 7(a). The simulated and measured reflection coefficients at one of the CB-CPW inputs of an antenna module are shown in Fig. 7(b). The measurement was made using 250 μm pitch GSG probes. The feed layer is facing up to allow for probing. The antenna layer faces down on a thick foam platform (no metal chuck underneath). The dielectric constant of foam is close to one, and it should only cause minor perturbation in the measurements [35], [36]. The measured reflection coefficient curve is shifted higher in frequency but other than that, a good agreement with the simulated curves is seen. The measured and simulated impedance bandwidths are 7.57 GHz and 9.75 GHz respectively, using the $|S_{11}| \leq -10$ dB criterion.

The transmission coefficients between *E*–*C*, *E*–*I*, *E*–*A*, and *E*–*G* were measured and simulated. The results in Fig. 8 show that the transmission $|S_{CE}|$ for the communicating pair *E*–*C* is generally higher than the transmission $|S_{IE}|$, $|S_{AE}|$, and $|S_{GE}|$ for the interfering pairs *E*–*I*, *E*–*A* and *E*–*G* across the band, for both measured and simulated values respectively. The differences in the levels of $|S_{CE}|$, $|S_{IE}|$, $|S_{AE}|$, and $|S_{GE}|$ are due to differences in the gain (i.e., main, back and side lobes) of *E* in the direction of *C*, *I*, *A*, and *G*. The main lobe level must be maximized while minimizing the back and SLLs in order to optimize the signal-to-interference ratio. A sensitivity analysis of the MAM with respect to the antenna parameters a_f, a_s and b was performed to take manufacturing tolerances into account [1]. With $a_f = a_s = 0.17$ mm and $b = 0.64$ mm, the simulated $|S_{CE}|$ (attainable) in Fig. 8(a) agrees much better with the measured curve. The space wave component of the simulated transmission for the *attainable*

case was estimated by performing another simulation of the MAM but after removing the intervening substrate and ground plane. The surface wave component can then be determined by subtraction [37]. As shown in Fig. 8(a), the surface waves have helped to increase transmission below 60 GHz.

VI. Conclusion

A 2-D Butler matrix integrated with a 60-GHz 2×2 circular patch planar array is demonstrated. The antenna module provides four switchable diagonal end-fire beams. A hybrid space-surface wave link is used for chip-to-chip communications. Five antenna modules are put together as the MAM to emulate interchip communication scenario in the MCMC system. The transmission between the communicating pair is higher than the interfering pairs. The surface waves in the link were shown to improve transmission below 60 GHz.

References

[1] P. Baniya, A. Bisognin, K. L. Melde, and C. Luxey, "Chip-to-chip switched beam 60 GHz circular patch planar antenna array and pattern considerations," *IEEE Trans. Antennas Propag.*, vol. 66, no. 4, pp. 1776–1787, Apr. 2018.

[2] P. Baniya and K. L. Melde, "Switched-beam end-fire planar array and integrated feed network for 60-GHz chip-to-chip space-surface wave communications," U.S. Patent Application 62 698 406, Jul. 16, 2018.

[3] H.-H. Yeh and K. L. Melde, "Development of 60-GHz wireless interconnects for interchip data transmission," *IEEE Trans. Compon. Packag. Manuf. Technol.*, vol. 3, no. 11, pp. 1946–1952, Nov. 2013.

[4] H.-H. Yeh, N. Hiramatsu, and K. L. Melde, "The design of broadband 60 GHz AMC antenna in multi-chip RF data transmission," *IEEE Trans. Antennas Propag.*, vol. 61, no. 4, pp. 1623–1630, Apr. 2013.

[5] A. Karkar, T. Mak, K.-F. Tong, and A. Yakovlev, "A survey of emerging interconnects for on-chip efficient multicast and broadcast in many-cores," *IEEE Circuits Syst. Mag.*, vol. 16, no. 1, pp. 58–72, 2016.

[6] L. Benini and G. De Micheli, "Networks on chips: A new SoC paradigm," *Computer*, vol. 35, no. 1, pp. 70–78, Jan. 2002.

[7] L. P. Carloni, P. Pande, and Y. Xie, "Networks-on-chip in emerging interconnect paradigms: Advantages and challenges," in *2009 3rd ACM/IEEE Int. Symp. Networks-on-Chip (NoC)*, San Diego, CA, USA, May 2009, pp. 93–102.

[8] G. M. Rebeiz, *RF MEMS Theory, Design, and Technology*. New York: Wiley, 2002.

[9] P. Baniya, S. Yoo, K. L. Melde, A. Bisognin, and C. Luxey, "Switched-beam 60-GHz four-element array for multichip multicore system," *IEEE Trans. Compon. Packag. Manuf. Technol.*, vol. 8, no. 2, pp. 251–260, Feb. 2018.

[10] G. H. Huff, J. Feng, S. Zhang, and J. T. Bernhard, "A novel radiation pattern and frequency reconfigurable single turn square spiral microstrip antenna," *IEEE Microw. Wireless Compon. Lett.*, vol. 13, no. 2, pp. 57–59, Feb. 2003.

[11] D. Rodrigo, T. Damgaci, B. A. Cetiner, J. Romeu Robert, and L. Jofre Roca, "MEMS-reconfigurable antenna based on a multi-size pixelled geometry," in *Proc. 4th Eur. Conf. Antennas Propag. (EuCAP)*, Barcelona, Spain, 2010, pp. 1–5.

[12] C.-H. Tseng, C.-J. Chen, and T.-H. Chu, "A low-cost 60-GHz switched-beam patch antenna array with Butler matrix network," *IEEE Antennas Wireless Propag. Lett.*, vol. 7, pp. 432–435, 2008.

[13] C.-C. Kuo, H.-C. Lu, P.-A. Lin, C.-F. Tai, Y.-M. Hsin, and H. Wang, "A fully SiP integrated V-band Butler matrix end-fire beam-switching transmitter using flip-chip assembled CMOS chips on LTCC," *IEEE Trans. Microw. Theory Tech.*, vol. 60, no. 5, pp. 1424–1436, May 2012.

[14] D. Titz, F. Ferrero, C. Luxey, G. Jacquemod, C. Laporte, and H. Ezzeddine, "Design of a miniaturized Butler matrix in IPD process for 60 GHz switched-beam antenna arrays," in *Proc. 2012 IEEE Int. Symp. Antennas Propag. (APSURSI)*, Chicago, IL, 2012, pp. 1–2.

[15] I. Ju *et al.*, "V-band beam-steering ASK transmitter and receiver using BCB-based system-on-package technology on silicon mother board," *IEEE Microw. Wireless Compon. Lett.*, vol. 21, no. 11, pp. 619–621, Nov. 2011.

[16] S. Lee *et al.*, "A V-band beam-steering antenna on a thin-film substrate with a flip-chip interconnection," *IEEE Microw. Wireless Compon. Lett.*, vol. 18, no. 4, pp. 287–289, Apr. 2008.

[17] W. Lee, J. Kim, C. S. Cho, and Y. J. Yoon, "Beamforming lens antenna on a high resistivity silicon wafer for 60 GHz WPAN," *IEEE Trans. Antennas Propag.*, vol. 58, no. 3, pp. 706–713, Mar. 2010.

[18] P. Ioannides and C. A. Balanis, "Uniform circular arrays for smart antennas," *IEEE Antennas Propag. Mag.*, vol. 47, no. 4, pp. 192–206, Aug. 2005.

[19] Y. Li and K.-M. Luk, "A multibeam end-fire magnetoelectric dipole antenna array for millimeter-wave applications," *IEEE Trans. Antennas Propag.*, vol. 64, no. 7, pp. 2894–2904, Jul. 2016.

[20] W. F. Moulder, W. Khalil, and J. L. Volakis, "60-GHz two-dimensionally scanning array employing wideband planar switched beam network," *IEEE Antennas Wireless Propag. Lett.*, vol. 9, pp. 818–821, 2010.

[21] Y. Li and K.-M. Luk, "60-GHz dual-polarized two-dimensional switch-beam wideband antenna array of aperture-coupled magneto-electric dipoles," *IEEE Trans. Antennas Propag.*, vol. 64, no. 2, pp. 554–563, Feb. 2016.

[22] J. Warnock *et al.*, "Circuit and physical design implementation of the microprocessor chip for the zEnterprise system," *IEEE J. Solid-State Circuits*, vol. 47, no. 1, pp. 151–163, Jan. 2012.

[23] K. Okada *et al.*, "Full four-channel 6.3-Gb/s 60-GHz CMOS transceiver with low-power analog and digital baseband circuitry," *IEEE J. Solid-State Circuits*, vol. 48, no. 1, pp. 46–65, Jan. 2013.

[24] H. Zhou, "High performance computing architecture with security," Ph.D. dissertation, Dept. Elect. Comput. Eng., Univ. Arizona, Tucson, AZ, USA, May 2015.

[25] C. A. Balanis, *Antenna Theory: Analysis and Design*, 3rd ed. Hoboken, NJ, USA: Wiley, 2005.

[26] *Rogers RO4400 Series Bondply Data Sheet: RO4450B and RO4450F Bondply*, Rogers Corp., Chandler, AZ, USA, 2018. [Online]. Available: http://www.rogerscorp.com

[27] *Rogers RO4003 Laminates Data Sheet*, Rogers Corp., Chandler, AZ, USA, 2018. [Online]. Available: http://www.rogerscorp.com

[28] S. Liao and Q. Xue, "Dual polarized planar aperture antenna on LTCC for 60-GHz antenna-in-package applications," *IEEE Trans. Antennas Propag.*, vol. 65, no. 1, pp. 63–70, Jan. 2017.

[29] D. G. Kam, D. Liu, A. Natarajan, S. K. Reynolds, and B. A. Floyd, "Organic packages with embedded phased-array antennas for 60-GHz wireless chipsets," *IEEE Trans. Compon. Packag. Manuf. Technol.*, vol. 1, no. 11, pp. 1806–1814, Nov. 2011.

[30] W. Hong, K.-H. Baek, and A. Goudelev, "Grid assembly-free 60-GHz antenna module embedded in FR-4 transceiver carrier board," *IEEE Trans. Antennas Propag.*, vol. 61, no. 4, pp. 1573–1580, Apr. 2013.

[31] D. Liu, J. A. G. Akkermans, H.-C. Chen, and B. Floyd, "Packages with integrated 60-GHz aperture-coupled patch antennas," *IEEE Trans. Antennas Propag.*, vol. 59, no. 10, pp. 3607–3616, Oct. 2011.

[32] C. Wang, E. Li, and D. F. Sievenpiper, "Surface-wave coupling and antenna properties in two dimensions," *IEEE Trans. Antennas Propag.*, vol. 65, no. 10, pp. 5052–5060, Oct. 2017.

[33] P. Baniya and K. L. Melde, "Link characteristics of directional surface wave antenna arrays," in *Proc. 12th Eur. Conf. Antennas Propag. (EuCAP)*, London, UK, to be published.

[34] ——, "Standing wave considerations in the link model of 60 GHz directional surface wave antenna arrays," in *Proc. 2018 IEEE Int. Symp. Antennas Propag. (APSURSI)*, Boston, MA, to be published.

[35] D. Titz, F. Ferrero, and C. Luxey, "Development of a millimeter-wave measurement setup and dedicated techniques to characterize the matching and radiation performance of probe-fed antennas [measurements corner]," *IEEE Antennas Propag. Mag.*, vol. 54, no. 4, pp. 188–203, Aug. 2012.

[36] P. Baniya, A. Bisognin, K. L. Melde, and C. Luxey, "Impact of gain and polarization in the design of reconfigurable chip-to-chip antennas," in *Proc. 10th Eur. Conf. Antennas Propag. (EuCAP)*, Davos, Switzerland, Apr. 2016, pp. 1–4.

[37] M. A. Khayat, J. T. Williams, D. R. Jackson, and S. A. Long, "Mutual coupling between reduced surface-wave microstrip antennas," *IEEE Trans. Antennas Propag.*, vol. 48, no. 10, pp. 1581–1593, Oct. 2000.